nature medicine

Fgf9 from dermal γδ T cells induces hair follicle neogenesis after wounding

Denise Gay[1,9], Ohsang Kwon[1,2,9], Zhikun Zhang[1], Michelle Spata[1], Maksim V Plikus[1,8], Phillip D Holler[1], Mayumi Ito[3], Zaixin Yang[1], Elsa Treffeisen[1], Chang D Kim[4], Arben Nace[1], Xiaohong Zhang[1], Sheena Baratono[1], Fen Wang[5], David M Ornitz[6], Sarah E Millar[1,7] & George Cotsarelis[1]

Understanding molecular mechanisms for regeneration of hair follicles provides new opportunities for developing treatments for hair loss and other skin disorders. Here we show that fibroblast growth factor 9 (Fgf9), initially secreted by γδ T cells, modulates hair follicle regeneration after wounding the skin of adult mice. Reducing Fgf9 expression decreases this wound-induced hair neogenesis (WIHN). Conversely, overexpression of Fgf9 results in a two- to threefold increase in the number of neogenic hair follicles. We found that Fgf9 from γδ T cells triggers Wnt expression and subsequent Wnt activation in wound fibroblasts. Through a unique feedback mechanism, activated fibroblasts then express Fgf9, thus amplifying Wnt activity throughout the wound dermis during a crucial phase of skin regeneration. Notably, humans lack a robust population of resident dermal γδ T cells, potentially explaining their inability to regenerate hair after wounding. These findings highlight the essential relationship between the immune system and tissue regeneration. The importance of Fgf9 in hair follicle regeneration suggests that it could be used therapeutically in humans.

The ability of skin to regenerate hair follicles during wound healing has been clearly shown in rodents[1,2]. In contrast, cutaneous wounds in adult humans typically result in fibrotic repair without regeneration of hair follicles. Investigators have speculated that the immune system is responsible for this scarring response, given that wound healing during fetal development, when the immune system is immature, leads to normal skin and hair follicle regeneration[3]. However, particularly in well-studied mouse models, the immune system is considered an important contributor to cutaneous wound healing. Specifically, epidermal γδ T cells produce factors, such as Fgf7, Fgf10 and IGF1, that are important for keratinocyte survival, proliferation and migration[4–6]. Here, we determined that dermal γδ T cells initiate an Fgf9-Wnt feedback loop necessary for hair follicle regeneration in wounds.

RESULTS

Fgf9 mediates wound-induced hair neogenesis

In the wound-induced hair neogenesis model, a 2.25 cm^2 full-thickness excisional wound is created on the backs of adult C57BL/6 mice. New hair follicle placodes appear after complete wound reepithelialization, which occurs at post-wound day 14 (PWD14, see **Fig. 1a** for WIHN timeline). Reasoning that important inductive events may occur before hair follicle placode formation, we compared gene expression profiles from whole skin during late wound healing. *Fgf9* was differentially expressed before hair follicle formation. We then used qPCR to show that *Fgf9* expression increased steadily in wound dermis during late healing but was not detected in the wound epidermis (**Fig. 1b**). These results show that *Fgf9* is upregulated in the wound dermis before the detection of new hair follicle placodes and potentially during a time of hair follicle fate determination.

To address the importance of Fgf9 in hair follicle neogenesis after wounding, we injected a neutralizing antibody to Fgf9 (anti-Fgf9) into the wound dermis every day for 4 d before hair follicle placode formation. Wounds treated with anti-Fgf9 showed a significant reduction ($P < 0.01$) in new hair follicle formation when compared with controls injected with an equal concentration of isotype-matched antibody (**Fig. 1c**). To test whether increased expression of *Fgf9* in the wound promotes WIHN, we overexpressed *Fgf9* in the epidermis of FVB-Tg(KRT14-rtTA)F42Efu/J; TRE-*Fgf9*-IRES-*EGFP* (K14rtTA; *Fgf9*) transgenic mice. Administration of doxycycline to these mice induces expression of *Fgf9* targeted to the epidermis by the promoter for the gene encoding keratin-14. *Fgf9* expression increased 150-fold in these mice after doxycycline administration (**Fig. 1d**), and this led to a marked increase in the number of neogenic hair follicles compared to controls (**Fig. 1e**,**f**). These combined results indicate that modulation of Fgf9 expression in the wound affects WIHN.

[1]Department of Dermatology, University of Pennsylvania, Philadelphia, Pennsylvania, USA. [2]Department of Dermatology, Seoul National University College of Medicine, Seoul, Korea. [3]Department of Dermatology, New York University Langone Medical Center, New York, New York, USA. [4]Department of Dermatology, School of Medicine, Chungnam National University, Daejeon, Korea. [5]Center for Cancer Biology and Nutrition, Institute of Biosciences and Technology, Texas A&M University Health Science Center, Houston, Texas, USA. [6]Department of Developmental Biology, Washington University School of Medicine, St. Louis, Missouri, USA. [7]Department of Cell and Developmental Biology, University of Pennsylvania, Philadelphia, Pennsylvania, USA. [8]Present address: Department of Developmental and Cell Biology, Sue and Bill Gross Stem Cell Research Center, University of California, Irvine, California, USA. [9]These authors contributed equally to this work. Correspondence should be addressed to G.C. (cotsarel@mail.med.upenn.edu).

Received 1 January; accepted 2 April; published online 2 June 2013; doi:10.1038/nm.3181

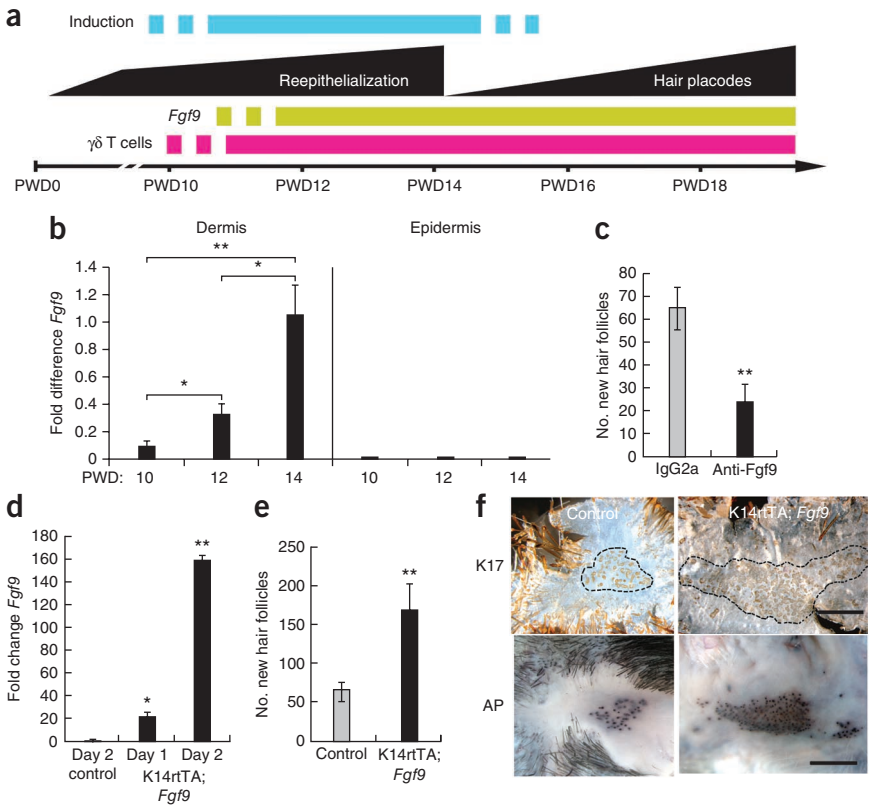

Figure 1 Fgf9 expression modulates WIHN. (**a**) Schematic model showing events in late-stage wound healing of normal mice aged 6–8 weeks. The blue bar specifies a hypothetical window of induction to hair follicle fate. (**b**) qPCR analyses of *Fgf9* expression in wound dermis and epidermis at PWD10–PWD14. cDNAs equalized for expression of the housekeeping gene 18S rRNA were compared for differences in *Fgf9* expression levels[30]. $n = 4$ for each time point. Results are representative of four independent experiments. (**c**) Number of new hair follicles in wounds of mice treated with anti-Fgf9 (black) or isotype control antibody (gray). Control mice: $n = 15$; mice treated with anti-Fgf9: $n = 16$. Data are representative of three independent experiments. (**d**) qPCR analyses of *Fgf9* expression in skin of K14rtTA; *Fgf9* mice compared to single-transgene controls (Control) during 2 d of doxycycline treatment. (**e**) Number of new hair follicles in wounds of K14rtTA; *Fgf9* transgenic (black) or control (gray) mice treated with doxycycline from PWD12 to PWD17. Single-transgene control mice: $n = 21$; K14rtTA; *Fgf9* transgenic mice: $n = 12$. Data are combined results from five independent experiments. (**f**) Whole-mount epidermal (top) or dermal (bottom) preparations of reepithelialized wounds stained for keratin 17 (K17, top) or alkaline phosphatase activity (AP, bottom). Black dashed line borders regions of new hair placodes. Scale bars, 1 mm. Data are expressed as means ± s.e.m. $^*P < 0.05$, $^{**}P < 0.01$ for panels **b**–**e**.

Dermal γδ T cells are the initial source of Fgf9

Peripheral blood γδ T cells are known to produce Fgf9 in humans[7]. To determine whether γδ T cells are the source of wound dermal Fgf9 and to determine their possible importance to WIHN, we studied the timing of entry of these cells into the wound dermis of C57BL/6 mice and engineered mice expressing eGFP in the nuclei of their γδ T cells (Tcrd-H2BEGFP mice[8]). γδ T cell numbers increased in the wound dermis just before the detection of *Fgf9* (**Fig. 2a**,**b**). Vγ3$^+$ dendritic epidermal T cells (Garman nomenclature), evident at the epidermal wound edge and in adjacent hair follicles, typically did not migrate far into the newly made wound epidermis or dermis (**Fig. 2a**). During the early period of γδ T cell entry into the wound (PWD9), most γδ T cells were dividing (**Fig. 2c**,**d**), suggesting that the wound environment provides important activation cues for these cells.

Vγ2$^+$ γδ T cells have been described as key contributors to inflammation in skin dermis[9,10]. Vγ4$^+$ γδ T cells are normal residents of nasal mucosa[11] and skin dermis (**Supplementary Fig. 1**). Our initial research showed that Vγ2$^+$ γδ T cells represent approximately 28% of normal back-skin γδ T cells and 5–10% of the wound-dermis γδ T cell population during late healing (**Fig. 2a**,**b**). Their reduced numbers in the wound suggested that they might not have a major role in late-stage wound healing. RT-PCR revealed both Vγ2$^+$ and Vγ4$^+$ T cell subtypes predominating in late-stage wounds (**Fig. 3a**).

To determine the source of Fgf9, we sorted PWD12 epidermal and dermal cells into three populations: major histocompatibility complex (MHC) class II–bearing cells (Langerhans cells, B cells, monocytes and macrophages), γδ T cells and double-negative cells (fibroblasts, αβ T cells, neutrophils and others). We sorted the dermal γδ T cell population further into Vγ2$^+$ and Vγ2$^-$ populations (**Fig. 3b**). We performed qPCR analyses of the sorted populations and found that dermal Vγ4$^+$ γδ T cells are the primary source of Fgf9 at this time point in wound healing (**Fig. 3b**). Double-negative cells also showed low levels of *Fgf9* expression, suggesting that an Fgf9-producing subpopulation exists within this group. Dendritic epidermal T cells were not an Fgf9 source. *In situ* hybridization localized *Fgf9* expression to γδ T cells within the wound dermis of Tcrd-H2BEGFP mice during this time period, supporting the qPCR results (**Fig. 3c**).

To determine whether γδ T cells have a role in WIHN, we wounded wild-type (WT) mice and mice lacking γδ T cells (*Tcrd*$^{-/-}$ mice). *Tcrd*$^{-/-}$ mice showed normal embryonic hair follicle development as determined by follicle morphology and number (**Supplementary Fig. 2** and data not shown). Wound healing times in *Tcrd*$^{-/-}$ mice lagged slightly (0.5–1 d) behind WT mice. This trend was much less notable than previously reported[4], probably owing to larger wound sizes and longer healing times.

Tcrd$^{-/-}$ mice showed significant defects in WIHN, with reductions of >60% in hair follicle numbers compared with WT controls ($P < 0.001$, **Fig. 3d**). To address the concern that γδ T cells may have a role in WIHN other than the production of Fgf9, we asked whether mice lacking Fgf9 specifically in T cells, including γδT cells, showed reduced WIHN. We first established by qPCR that γδ T cells are the only T cell source of Fgf9 in the wound (**Supplementary Fig. 3**). Transgenic mice lacking Fgf9 in T cells (*Lck-Cre*; *Fgf9*$^{fl/fl}$) showed markedly fewer new hair follicles compared to single transgene controls, comparable to the reduction of WIHN in *Tcrd*$^{-/-}$ mice (**Fig. 3e**,**f**). These mice showed healing times comparable to WT and heterozygous littermates. These combined results demonstrate that Fgf9, expressed by γδ T cells in the late wound dermis, is an important contributor to WIHN.

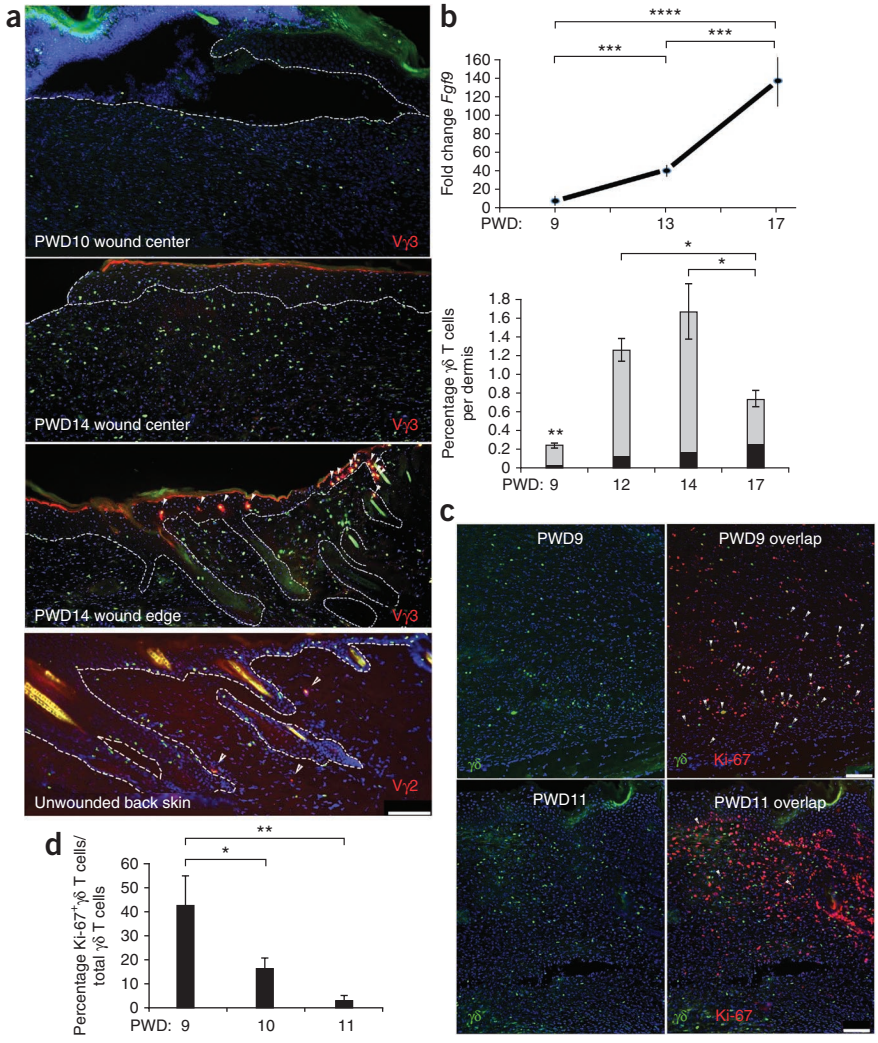

Figure 2 Kinetics of γδ T cell density and *Fgf9* expression in wound dermis during late healing and in unwounded skin. (**a**) Immunofluorescence (IF) analyses of wounded and unwounded Tcrd-H2BEGFP skin frozen sections stained with antibodies to detect Vγ3$^+$ dendritic epidermal T cells (red) in wound center (top, middle) and wound edge (second from bottom, arrowheads) at PWD10 or PWD14 as indicated or Vγ2$^+$ T cells in unwounded skin (bottom, arrowheads). Green nuclei denote γδ T cells. DAPI staining (blue) shows the locations of all nuclei. Dashed lines represent the junction between epidermis and dermis. Scale bar, 100 μm. Vγ2$^+$GFP$^+$ cells in multiple sections indicated that they represent approximately 28% of dermal γδ T cells in unwounded back skin (data not shown). $n = 8$. Results are representative of four independent experiments. (**b**) qPCR analyses of *Fgf9* expression (top) compared with percentage of γδ T cells (bottom, gray) and percentage of Vγ2$^+$ γδ T cells (black) per C57BL/6 wound dermis from PWD9 to PWD17 as determined by FACS. $n = 20$ for each time point. (**c**) IF analyses showing γδ T cells (left) and Ki-67$^+$ γδ T cells (right, arrowheads) within PWD9 (top) and PWD11 (bottom) Tcrd-H2BEGFP wounds. Scale bar, 100 μm. (**d**) Percentage of Ki-67$^+$ γδ T cells per total number γδ T cells as counted in sequential frozen sections of Ki-67–specific antibody–stained *Tcrd-H2BEGFP* PWD9–PWD11 wounds. $n = 6$–20 for each time point. Results are representative of four independent experiments. Data are expressed as means ± s.e.m. $^*P < 0.05$, $^{**}P < 0.01$, $^{***}P < 0.005$, $^{****}P < 0.001$ for **b** (γδ T cells only) and **d**.

reepithelialization and dermal remodeling and in similar time frames (**Fig. 4a**,**b**).

We previously showed that forced overexpression of Wnt7a in epidermis of the *Krt14-Wnt7a* mouse leads to markedly more WIHN compared to WT controls[1]. To determine whether overexpression of Wnt7a in the epidermis could rescue WIHN in our model, we analyzed *Krt14-Wnt7a*; *Tcrd*$^{-/-}$ (*Wnt7a*; *Tcrd*$^{-/-}$) mice and controls for WIHN. As previously reported, wounds of *Krt14-Wnt7a* (*Wnt7a*) control mice had large numbers of new hair follicles[1] (**Fig. 4d**,**e**). In marked contrast, wounds of *Wnt7a*; *Tcrd*$^{-/-}$ mice showed significantly less WIHN ($P < 0.01$). This result was surprising because, in embryonic hair follicle development, overlying epidermis provides the necessary Wnt source for dermal Wnt activation[14]. However, because dermal Wnt activity preceded reepithelialization in the wound (see **Fig. 4a**), epidermal Wnt might arrive too late to rescue the phenotype in this model. In support of this, PWD12 wound dermis of *Wnt7a*; *Axin2-LacZ* mice showed no difference in *Axin2* expression, and therefore in dermal Wnt activity, compared with that of *Axin2-LacZ* mice (**Fig. 4f**). As expected, amplified Wnt activity was observed in the surrounding unwounded skin of *Wnt7a*; *Axin2-LacZ* mice (**Fig. 4f**).

To address whether Fgf9 could rescue WIHN in mice lacking γδ T cells, we injected adenovirus containing either an *Fgf9* construct (AdFgf9) or a control *GFP* construct (AdGFP) into the PWD9 dermis of *Axin2-LacZ*; *Tcrd*$^{-/-}$ mice. Augmented *Axin2* expression was observed in AdFgf9-treated but not AdGFP-treated wounds at PWD12 (**Fig. 4g**). Analysis of WIHN showed a significantly higher number of

Fgf9 promotes dermal Wnt activation that induces WIHN

Fgf9 has been shown to activate canonical Wnt signaling during lung development through the induction of Wnt expression by mesenchymal cells[12,13]. We reasoned that Fgf9 may induce Wnt activation in the wound. Analysis of dermal Wnt activation in wounds of Wnt-reporter mice (*Axin2-LacZ* heterozygotes) revealed increased activity in late-stage wounds with abatement around PWD16 when Axin2 concentrated predominantly in new hair follicle placodes of the epithelium (**Fig. 4a**). Analyses of PWD12 dermis for nuclear β-catenin and Lef1, other important indicators of Wnt activity, confirmed results observed in wounds of *Axin2-LacZ* mice (**Supplementary Fig. 4**). These data indicate that dermal Wnt activation is a component of late healing and, as in embryonic development, a key first step for hair follicle neogenesis[14].

To test the hypothesis that Fgf9 from γδ T cells is the catalyst for dermal Wnt activation, *Axin2-LacZ*; *Tcrd*$^{-/-}$ mice were wounded and analyzed for Axin2-LacZ expression (**Fig. 4a**,**b**). Axin2-LacZ expression in *Tcrd*$^{-/-}$ PWD12 dermis and PWD14 epidermis and dermis was markedly reduced compared to control *Axin-LacZ* mice. qPCR confirmed that wound dermis of *Tcrd*$^{-/-}$ mice had reduced expression of *Axin2* and *Lef1* compared to WT controls (**Fig. 4c**). Reduced Axin2 expression did not appear to affect healing, as wounds of both WT and *Tcrd*$^{-/-}$ mice showed comparable

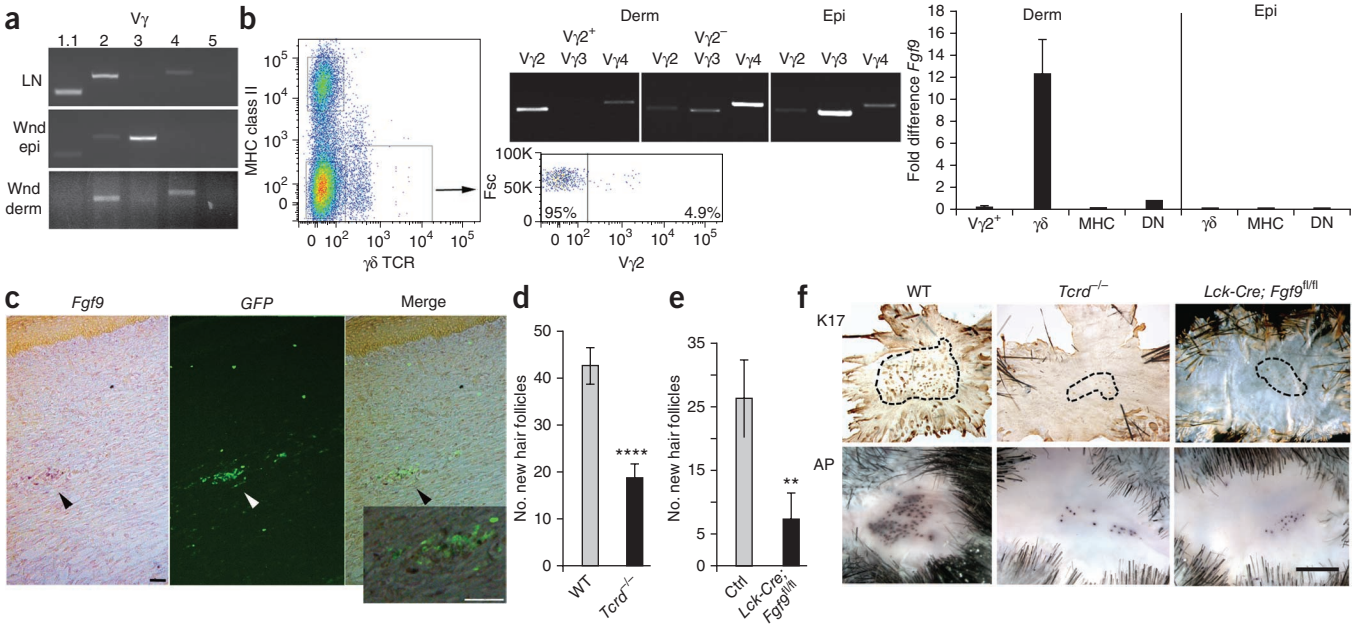

Figure 3 Fgf9, secreted by wound dermal γδ T cells, is an important component of WIHN. (**a**) RT-PCR analyses of lymph node cells (LN), wound epidermis (Wnd epi) and wound dermis (Wnd derm) for rearranged Vγ variable regions Vγ1.1, Vγ2, Vγ3, Vγ4 and Vγ5 ($n = 4$). Results are representative of three independent experiments. (**b**) Left, pseudocolor density dot plot of PWD12 dermal cells sorted for expression of MHC class II and γδ TCR. The lower boxed population represents cells that were further sorted for Vγ2 expression (right dot plot) and forward scatter (Fsc). Middle, RT-PCR analysis of sorted Vγ2$^+$ and Vγ2$^-$ populations from dermis (Derm) and sorted γδ T cells from wound epidermis (Epi) for Vγ2, Vγ3 and Vγ4 to determine purity of each population. Right, qPCR analyses of sorted Vγ2$^+$ γδ T cells (Vγ2$^+$), all other γδ T cells (γδ), MHC class II$^+$ cells (MHC) and nonstaining double-negative cells (DN) in wound dermis (left) or γδ, MHC and double-negative cells in wound epidermis (right) for *Fgf9* expression. For these experiments, wound dermis or epidermis from 20–40 mice was combined and sorted. Results are representative of three independent experiments. (**c**) *In situ* hybridization for *Fgf9* expression in a Tcrd-H2BEGFP wound frozen section. Left image (*Fgf9*) shows *in situ* hybridization for *Fgf9* expression in a PWD11 frozen section. Dark purple dots (black arrowhead) represent *Fgf9*$^+$ cells in the dermis. Middle image (*GFP*) shows location of *GFP*-expressing γδ T cells (white arrowhead) within the same section. Right image (Merge) shows overlap of left and middle images. Scale bar, 75 μm. The inset represents a magnified view of the region indicated by the black arrowhead in right image. Scale bar, 75 μm ($n = 12$). Results are representative of four independent experiments. Probe specificity is illustrated in **Supplementary Figure 7b**. (**d**) Number of new hair follicles in wounds of WT control and *Tcrd*$^{-/-}$ mice. WT mice: $n = 37$; *Tcrd*$^{-/-}$ mice: $n = 50$. Data represent combined results of eight independent experiments. (**e**) Number of new hair follicles in wounds of *Lck-Cre*; *Fgf9*$^{fl/fl}$ and control (Ctrl) mice. *Lck-Cre*; *Fgf9*$^{fl/fl}$ mice: $n = 17$; single-transgene control mice: $n = 30$. Data represent combined results of seven independent experiments. (**f**) Representative whole-mount preparations of wound epidermis from WT, *Tcrd*$^{-/-}$ and *Lck-Cre*; *Fgf9*$^{fl/fl}$ mice stained for Keratin 17 (K17) and dermis stained for alkaline phosphatase activity (AP). Black dashed lines represent borders of areas with new hair placodes. Scale bar, 1 mm. Data are expressed as means ± s.e.m. $^{**}P < 0.01$, $^{****}P < 0.001$ compared to controls, calculated using two-tailed Student's *t* test.

new hair follicles in AdFgf9-treated mice ($P < 0.05$, **Fig. 4h**). These data confirm that exogenous Fgf9 can induce Wnt activity in wounds and positively influence WIHN. Because treatment did not fully restore WIHN, other, as yet unknown, γδ T cell–mediated effects may also affect WIHN.

Fgf9 from γδ T cells initiates a feedback loop

During lung development, Fgf9 induces canonical Wnt2a ligand expression in mesenchymal cells[12]. In initial experiments, we found that Wnt2a was expressed in normal wound dermis and reduced in *Tcrd*$^{-/-}$ dermis, suggesting that Wnt2a might also have a role in wound healing (**Fig. 4b**,**c**). Reasoning that wound fibroblasts might be the target of Fgf9 activation, we first established that FgfR2 and FgfR3, both high affinity receptors for Fgf9 (ref. 15), were present in fibroblasts from WT and *Tcrd*$^{-/-}$ wound dermis (**Supplementary Fig. 5**). We then cultured wound fibroblasts in the presence or absence of Fgf9 and evaluated expression of *Wnt2* and an unrelated canonical Wnt (*Wnt10a*). Fibroblasts cultured with exogenous Fgf9 expressed substantially higher levels of *Wnt2* but not *Wnt10a* transcripts (**Fig. 5a**). *Tcrd*$^{-/-}$ fibroblasts showed similar results, indicating that these cells are capable of *Wnt2* expression if provided with Fgf9.

We also compared sorted wound fibroblasts from WT mice and *Tcrd*$^{-/-}$ mice for *Wnt2* expression during late healing (**Fig. 5b**) (the sorting strategy for fibroblasts is found in Online Methods and **Supplementary Fig. 6**). WT wound fibroblasts, but not *Tcrd*$^{-/-}$ fibroblasts, showed an increase in *Wnt2* expression over time. These results further support a role for γδ T cell–secreted Fgf9 in the induction of *Wnt2* by fibroblasts and subsequent Wnt activation *in vivo*.

Unexpectedly, sorted WT fibroblasts, but not *Tcrd*$^{-/-}$ fibroblasts, also showed increased expression of *Fgf9* (**Fig. 5b**). To determine when fibroblasts initiated *Fgf9* gene expression compared to γδT cells *in vivo*, we established a timeline of *Fgf9* expression for both (**Fig. 5c**). Comparisons showed that early in this window, γδT cells were the primary source of Fgf9 in the wound, but fibroblasts had higher Fgf9 expression during later healing. *In situ* hybridization comparing *Fgf9* expression in PWD11, PWD12 and PWD14 wounds supported this finding (**Supplementary Fig. 7**). Because WT, but not *Tcrd*$^{-/-}$, fibroblasts showed upregulation of *Fgf9* expression *in vivo* (1–2 d after γδ T cell *Fgf9* expression), we reasoned that this new gene expression might be a consequence of Wnt activation.

Fgf9 has been shown as a canonical Wnt target in endometrioid adenocarcinomas[16]. To address the possibility that *Fgf9* is a Wnt target

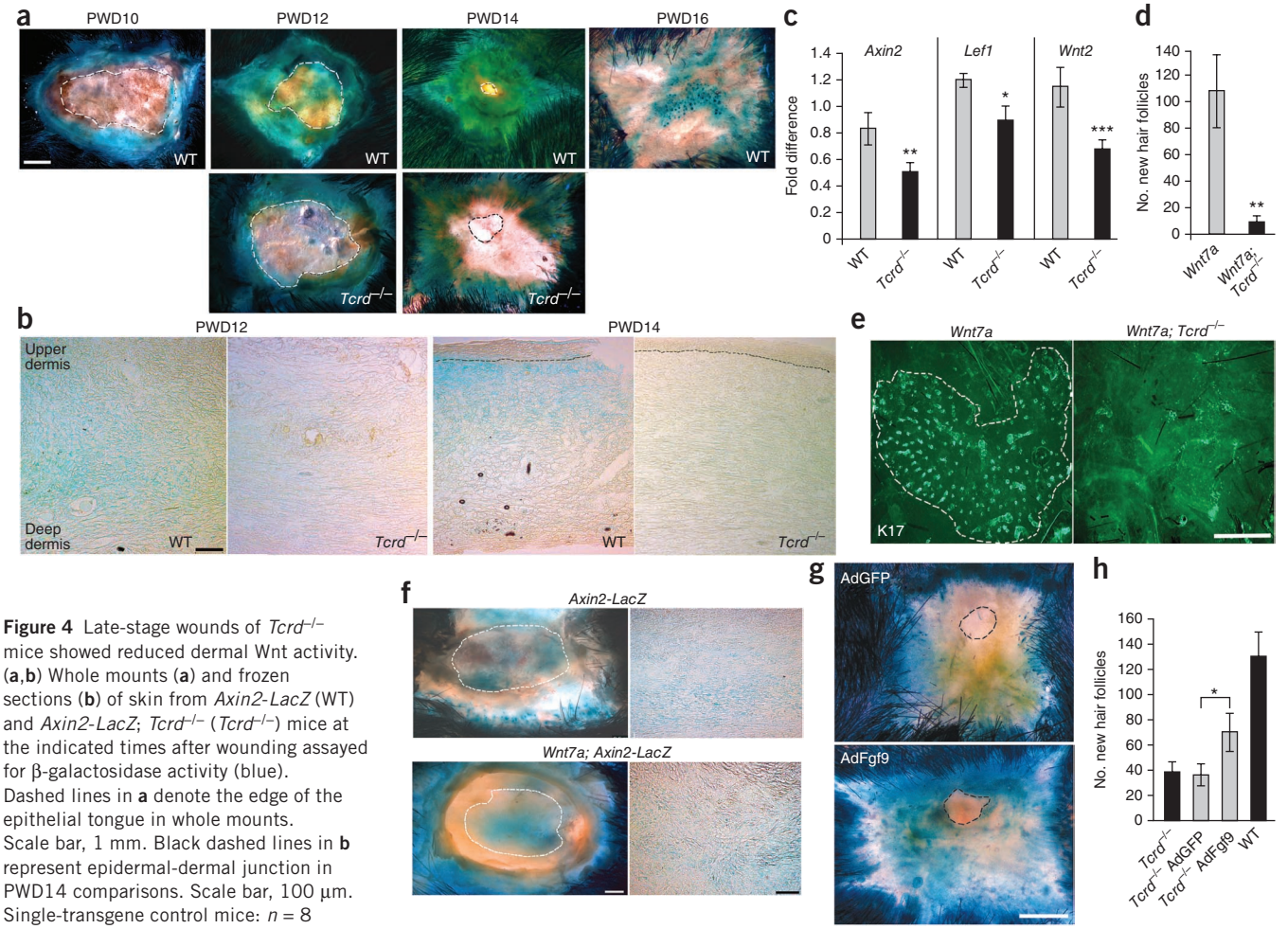

Figure 4 Late-stage wounds of *Tcrd*$^{-/-}$ mice showed reduced dermal Wnt activity. (**a**,**b**) Whole mounts (**a**) and frozen sections (**b**) of skin from *Axin2-LacZ* (WT) and *Axin2-LacZ*; *Tcrd*$^{-/-}$ (*Tcrd*$^{-/-}$) mice at the indicated times after wounding assayed for β-galactosidase activity (blue). Dashed lines in **a** denote the edge of the epithelial tongue in whole mounts. Scale bar, 1 mm. Black dashed lines in **b** represent epidermal-dermal junction in PWD14 comparisons. Scale bar, 100 μm. Single-transgene control mice: $n = 8$ (PWD10), $n = 22$ (PWD12), $n = 12$ (PWD14), $n = 6$ (PWD16); *Axin2-LacZ*; *Tcrd*$^{-/-}$ mice: $n = 14$ (PWD12), $n = 7$ (PWD14). Data are representative of six independent experiments. (**c**) Relative expression of *Axin2*, *Lef1* and *Wnt2* in wound dermis of C57BL/6 (WT) and *Tcrd*$^{-/-}$ mice as determined by qPCR. WT mice: $n = 12$; *Tcrd*$^{-/-}$ mice: $n = 12$. Data are representative of three independent experiments. (**d**) Number of new hair follicles in wounds of *Krt14-Wnt7a* (*Wnt7a*) and *Krt14-Wnt7a*; *Tcrd*$^{-/-}$ (*Wnt7a*; *Tcrd*$^{-/-}$) mice. *Wnt7a* mice: $n = 9$; *Wnt7a*; *Tcrd*$^{-/-}$ mice: $n = 20$. Data are combined results from four independent experiments. (**e**) Representative whole-mount preparations of wound epidermis from *Krt14-Wnt7a* (*Wnt7a*) and *Krt14-Wnt7a*; *Tcrd*$^{-/-}$ (*Wnt7a*; *Tcrd*$^{-/-}$) mice immunostained for K17. The white dashed line in the left image represents the border of new hair placodes. Scale bar, 0.5 mm. (**f**) Whole mounts (left) and frozen sections (right) from wounds of *Axin2-LacZ* (top) and K14-*Wnt7a*; *Axin2-LacZ* (*Wnt7a*; *Axin2-LacZ*, bottom) mice assayed for β-galactosidase activity at PWD12. Left; white dashed line denotes the edge of the epithelial tongue. Scale bar, 1 mm. Right; scale bar, 100 μm ($n = 4$). Results are representative of three independent experiments. (**g**) Representative whole-mount preparations from wounds of *Axin2-LacZ*; *Tcrd*$^{-/-}$ mice injected with AdGFP (top) or AdFgf9 (bottom) at PWD9 and assayed for β-galactosidase activity at PWD12. The dashed lines denote the edge of the epithelial tongue. Scale bar, 1 mm. (**h**) Number of new hair follicles in untreated wounds of *Axin2-LacZ*; *Tcrd*$^{-/-}$ (far left, black) and *Axin2-LacZ* WT (far right, black) mice or wounds of AdGFP-injected (left, gray) and AdFgf9-injected (right, gray) *Axin2-LacZ*; *Tcrd*$^{-/-}$ mice. Untreated *Axin2-LacZ*; *Tcrd*$^{-/-}$ mice: $n = 12$; untreated *Axin2-LacZ* WT mice: $n = 18$; AdGFP-treated mice: $n = 25$; AdFgf9-treated mice: $n = 25$. Data are representative of seven independent experiments. Data are expressed as means ± s.e.m. $^{*}P < 0.05$, $^{**}P < 0.01$, $^{***}P < 0.005$.

in wounds, we cultured dermal wound fibroblasts with increasing amounts of recombinant Wnt2a protein over 3 d. Culture supernatants, when tested for Fgf9 protein by ELISA, showed increasing expression of Fgf9 over time (**Fig. 5d**). These data reveal *Fgf9* as a target of Wnt activation in wound fibroblasts.

These combined data show that Fgf9, secreted by γδ T cells during PWD10–12, acts as the catalyst for regional dermal fibroblast Wnt2a expression and subsequent Wnt activation (**Fig. 5e**). In turn, this activation induces further expression of Fgf9 from fibroblasts, which serves to perpetuate and amplify Wnt activation throughout the entire dermis during a crucial phase for WIHN. Although others have shown the ability of Fgf9 to induce Wnt activation[12,13] and Wnt activation to induce expression of Fgf9 (ref. 16), to our knowledge, these data are the first to link these important signaling cascades in an amplification loop (**Fig. 5e**).

Humans lack a robust population of dermal γδ T cells

Humans lack appreciable hair follicle regeneration after wounding compared to mice. To understand whether differences in immune cells may explain this deficiency, we compared relative numbers and locations of γδ T cells within the dermis of normal mouse and human skin (**Fig. 6**). In line with other work[9,17–22], we found that human dermis showed a notable paucity of resident γδ T cells in number and density per area compared with mouse dermis (**Fig. 6a–d**).

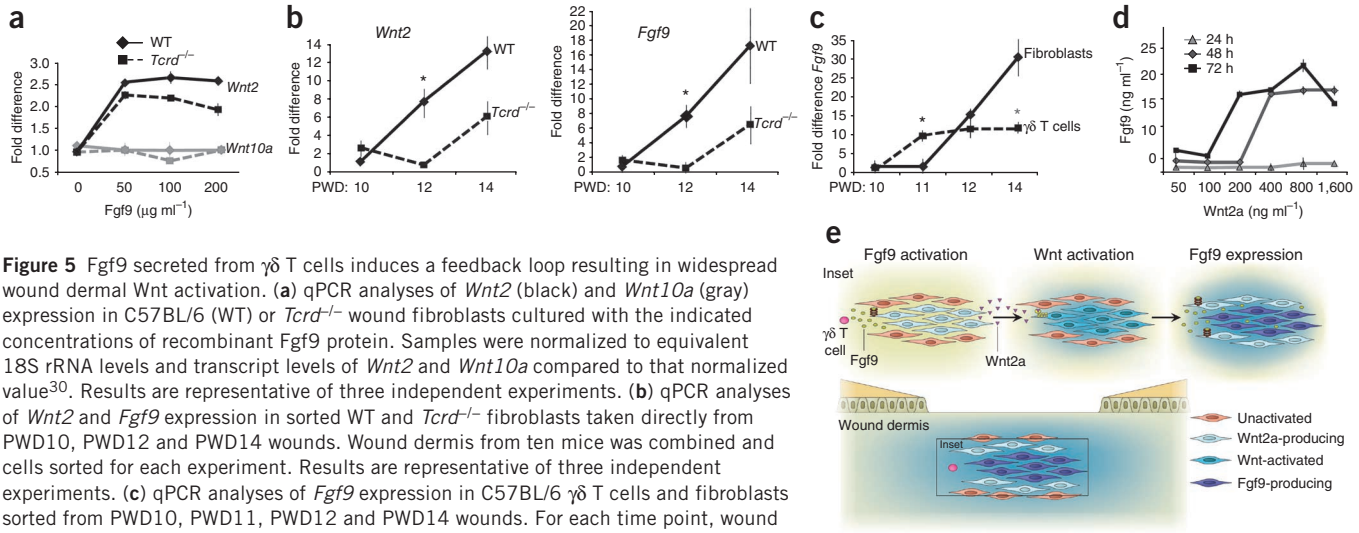

Figure 5 Fgf9 secreted from γδ T cells induces a feedback loop resulting in widespread wound dermal Wnt activation. (**a**) qPCR analyses of *Wnt2* (black) and *Wnt10a* (gray) expression in C57BL/6 (WT) or *Tcrd*$^{-/-}$ wound fibroblasts cultured with the indicated concentrations of recombinant Fgf9 protein. Samples were normalized to equivalent 18S rRNA levels and transcript levels of *Wnt2* and *Wnt10a* compared to that normalized value[30]. Results are representative of three independent experiments. (**b**) qPCR analyses of *Wnt2* and *Fgf9* expression in sorted WT and *Tcrd*$^{-/-}$ fibroblasts taken directly from PWD10, PWD12 and PWD14 wounds. Wound dermis from ten mice was combined and cells sorted for each experiment. Results are representative of three independent experiments. (**c**) qPCR analyses of *Fgf9* expression in C57BL/6 γδ T cells and fibroblasts sorted from PWD10, PWD11, PWD12 and PWD14 wounds. For each time point, wound dermis from 10–15 mice was combined and sorted. Results represent three independent experiments. $^{*}P < 0.05$. (**d**) ELISA analyses of secreted Fgf9 protein from wound fibroblasts of *Axin2-LacZ* mice, cultured with the indicated concentrations of recombinant Wnt2a protein for 24 h, 48 h and 72 h. Results are representative of three independent experiments. (**e**) Model depicting Fgf9-driven Wnt activation feedback loop. Boxed region in the bottom image (inset) shows the dermal location of fibroblasts undergoing Fgf9 activation and Wnt2a expression (top left), Wnt activation (top middle) and new Fgf9 expression (top right). Data are expressed as means ± s.e.m.

We also noted a difference in location of mouse and human dermal γδ T cells. Mouse γδ T cells were dispersed throughout the dermis, typically away from αβ T cells and blood vessels (**Fig. 6e**,**f**). In contrast, human γδ T cells clustered with αβ T cells in vascularized dermal 'pockets' (**Fig. 6e**,**f**), suggesting that they transit between skin and blood at least infrequently. The low number and sequestered location of γδ T cells in human compared to mouse skin may explain the poor regenerative response of human skin to wounding.

DISCUSSION

Wnt signaling pathways used for hair follicle development are mirrored in WIHN. We showed previously that epidermal Wnt activation is a necessary component of WIHN, as it is for hair follicle development[1,23,24]. Here, we show that early dermal Wnt activation is also requisite for hair follicle regeneration. Indeed, this model provides an opportunity to uncouple epidermal and dermal contributions to hair follicle regeneration because overlying epidermis is absent during

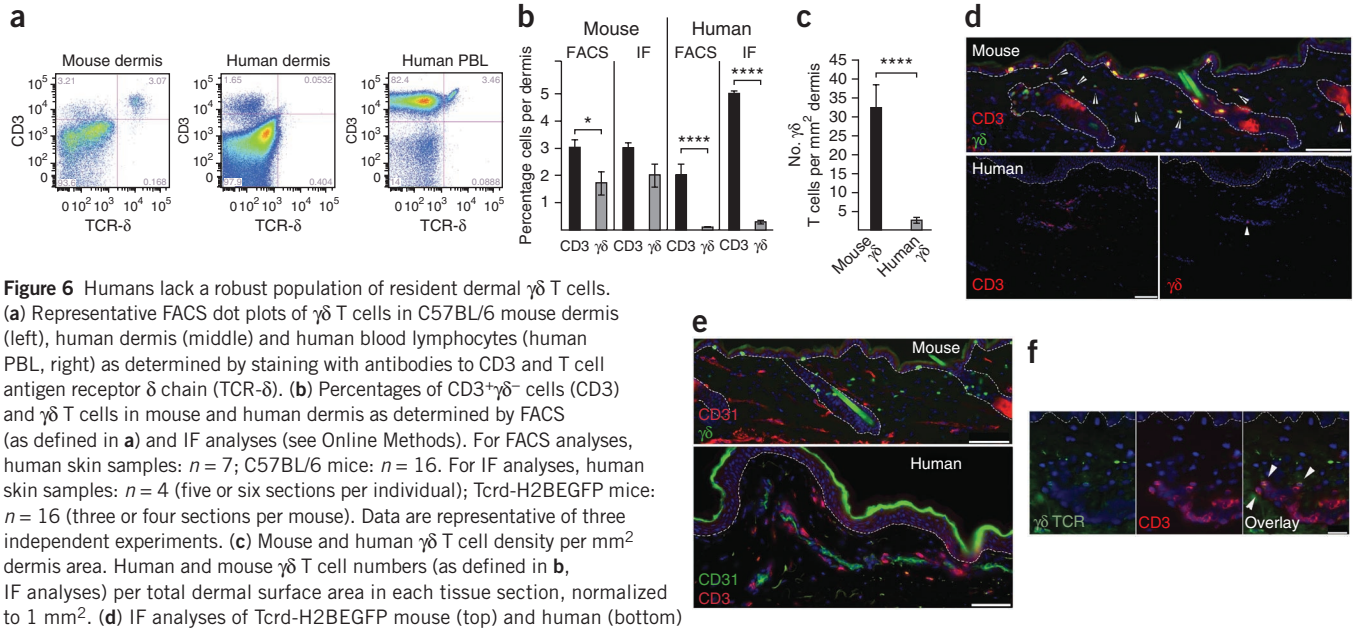

Figure 6 Humans lack a robust population of resident dermal γδ T cells. (**a**) Representative FACS dot plots of γδ T cells in C57BL/6 mouse dermis (left), human dermis (middle) and human blood lymphocytes (human PBL, right) as determined by staining with antibodies to CD3 and T cell antigen receptor δ chain (TCR-δ). (**b**) Percentages of CD3^{+}γδ^{-} cells (CD3) and γδ T cells in mouse and human dermis as determined by FACS (as defined in **a**) and IF analyses (see Online Methods). For FACS analyses, human skin samples: $n = 7$; C57BL/6 mice: $n = 16$. For IF analyses, human skin samples: $n = 4$ (five or six sections per individual); Tcrd-H2BEGFP mice: $n = 16$ (three or four sections per mouse). Data are representative of three independent experiments. (**c**) Mouse and human γδ T cell density per mm^2 dermis area. Human and mouse γδ T cell numbers (as defined in **b**, IF analyses) per total dermal surface area in each tissue section, normalized to 1 mm^2. (**d**) IF analyses of Tcrd-H2BEGFP mouse (top) and human (bottom) skin frozen sections showing locations of CD3^{+} T cells and γδ T cells (arrowheads). DAPI-stained nuclei are blue. Dashed lines represent dermal-epidermal junction. Scale bars, 75 μm. (**e**) IF analyses of Tcrd-H2BEGFP mouse (top) and human (bottom) skin locations of γδ T cells (green, top), CD3^{+} T cells (red, bottom) relative to CD31^{+} blood vessels. Dashed lines represent dermal-epidermal junction. Scale bars, 75 μm. (**f**) IF analyses of human skin γδ T cells (green, left), all CD3^{+} T cells (red, middle) and merged image (right, arrowheads point to γδ T cells). Dashed white line represents dermal-epidermal junction. Scale bar, 25 μm. For panels **b** and **c**, data are expressed as means ± s.e.m. $^{*}P < 0.05$, $^{****}P < 0.001$ compared to controls, calculated using two-tailed Student's *t* test.

initial dermal Wnt activation. Also, overexpression of epidermal Wnt after reepithelialization does not contribute to dermal Wnt activation and is insufficient to trigger WIHN.

During embryogenesis, dermal Wnt activation has been known as an early event in skin maturation and postulated as the first signal for hair induction[24,25]. However, only recently has this hypothesis been formally substantiated. In the absence of either epidermal Wnts[14,26] or dermal Wnt activation[14], hair follicle placodes did not form, designating Wnt activation as an essential early step in hair follicle development.

In the wound, we have shown that γδ T cells produce Fgf9, which induces fibroblast Wnt expression, ultimately leading to WIHN. In development, the upstream signal driving Wnt expression in epidermis remains unknown. Recently, Fgf20, a member of the Fgf9 family, was implicated in feather-placode induction in chickens[27]. The scaleless mutation, manifested by the complete lack of patterned placode formation and subsequent feathers, has been mapped to the gene encoding Fgf20 (refs. 27,28). In the mouse, however, genetic loss of *Fgf20* permits placode but not guard hair dermal condensate formation, thus pointing to a function downstream of placode specification[29]. Indeed, these mice lack guard hairs but maintain other hair types, albeit at lower densities. These results suggest possible redundancy with other Fgf9 family members in inducing early epidermal Wnt expression in mice. Alternatively, mechanisms other than Fgf signaling may serve to upregulate mouse epidermal Wnts during skin development.

Although dermal Wnt activation is necessary for hair follicle development and regeneration, its role remains unknown. Chen *et al.*[14] showed fibroblast proliferation after dermal Wnt activation, and we have noted considerable dermal proliferation in wounds during late healing (**Supplementary Fig. 1c**). However, fibroblast proliferation probably reveals only a part of the story. In development and late healing, epidermal Wnt activation closely follows dermal activation. Chen *et al.*[14] proposed that dermal Wnt activation drives epidermal Wnt activation, presumably through a soluble dermal 'factor'. In WIHN, we showed that wound fibroblasts secrete Wnts in response to Fgf9-mediated cues. Increased Wnt expression in the dermis may augment epidermal Wnt concentrations, overcoming a threshold for triggering epidermal activation and hair follicle formation. In embryogenesis, Wnts and Wntless, a cargo protein required for Wnt secretion, are expressed in both early embryonic epidermis and dermis[25,26]. However, loss of dermal Wntless does not seem to affect epidermal Wnt activity or the subsequent development of hair follicles, suggesting other, as yet unknown, mechanisms[14].

As outlined above, early signaling pathways for hair follicle induction in development and WIHN are probably the same. However, the cells that drive these induction events are different. γδ T cells provide initial Fgfs for Fgf signaling and fibroblasts provide Wnts for dermal Wnt activation in WIHN, whereas the epidermis probably provides these factors in development. These examples illustrate the parallels and important differences between skin development and regeneration in response to wounding and demonstrate the positive impact of the immune system on tissue renewal.

Our Fgf9 overexpression studies support the notion that wounding produces a window of opportunity to push regenerating epidermis toward a hair follicle fate. The introduction of AdFgf9 to γδ T cell–deficient mouse skin during wounding compensated for lack of Fgf9 and resulted in increased numbers of hair follicles, thus indicating the potential for using Fgf9 to manipulate hair follicle regeneration. Future studies testing activators of the Fgf or Wnt pathways during wound healing may be warranted to determine their effects on hair follicle regeneration. This avenue of research could lead to new approaches for promoting hair growth in patients with hair loss.

METHODS

Methods and any associated references are available in the online version of the paper.

Note: Supplementary information is available in the online version of the paper.

ACKNOWLEDGMENTS

We thank R.L. O'Brien for thoughtful reading of the manuscript, P. Coulombe (Johns Hopkins University) for providing K17-specific antisera and members of A. Bhandoola's laboratory and The University of Pennsylvania Flow Cytometry and Cell Sorting Resource Laboratory for assistance with cell-sorting experiments. We also thank J. Tobias and D. Baldwin of the Penn Microarray Core Facility, L. Ash of the Dermatology Department Histology Core and the Penn Human Cooperative Tissue Network. Funding was provided by US National Institutes of Health (NIH) grant R01-AR46837, NIH Skin Diseases Research Core grant P30-AR057217, the Edwin and Fannie Gray Hall Center for Human Appearance at University of Pennsylvania Medical Center and The Dermatology Foundation. This work was also supported by NIH grant 5RO1 AR055309-4 and, for D.M.O., grant R01 HL105732. P.D.H. is supported by NIH training grant 5T32AR007465-29.

AUTHOR CONTRIBUTIONS

D.G., O.K. and G.C. designed the studies and analyzed and interpreted the results with assistance from Z.Z., M.S., P.D.H., Z.Y., E.T., C.D.K., A.N., X.Z. and S.B. D.G. wrote and D.G and G.C. edited the manuscript. M.V.P., P.D.H., M.I., F.W., D.M.O. and S.E.M. provided theoretical and technical advice and assistance. F.W. and D.M.O. provided TRE-*Fgf9*-IRES-*EGFP* and $Fgf9^{fl/fl}$ mice, and S.E.M. provided *Krt14-Wnt7a* mice. D.M.O. provided pGEM-Fgf9 plasmid.

COMPETING FINANCIAL INTERESTS

The authors declare competing financial interests: details are available in the online version of the paper.

1. Ito, M. *et al.* Wnt-dependent de novo hair follicle regeneration in adult mouse skin after wounding. *Nature* **447**, 316–320 (2007).
2. Breedis, C. Regeneration of hair follicles and sebaceous glands from the epithelium of scars in the rabbit. *Cancer Res.* **14**, 575–579 (1954).
3. Gurtner, G.C., Werner, S., Barrandon, Y. & Longaker, M.T. Wound repair and regeneration. *Nature* **453**, 314–321 (2008).
4. Jameson, J. *et al.* A role for skin γδ T cells in wound repair. *Science* **296**, 747–749 (2002).
5. Sharp, L.L., Jameson, J.M., Cauvi, G. & Havran, W.L. Dendritic epidermal T cells regulate skin homeostasis through local production of insulin-like growth factor 1. *Nat. Immunol.* **6**, 73–79 (2005).
6. Toulon, A. *et al.* A role for human skin-resident T cells in wound healing. *J. Exp. Med.* **206**, 743–750 (2009).
7. Workalemahu, G., Foerster, M. & Kroegel, C. Expression and synthesis of fibroblast growth factor-9 in human γδ T lymphocytes. Response to isopentenyl pyrophosphate and TGF-β1/IL-15. *J. Leukoc. Biol.* **75**, 657–663 (2004).
8. Prinz, I. *et al.* Visualization of the earliest steps of γδ T cell development in the adult thymus. *Nat. Immunol.* **7**, 995–1003 (2006).
9. Cai, Y. *et al.* Pivotal role of dermal IL-17–producing γδ T cells in skin inflammation. *Immunity* **35**, 596–610 (2011).
10. Sumaria, N. *et al.* Cutaneous immunosurveillance by self-renewing dermal γδ T cells. *J. Exp. Med.* **208**, 505–518 (2011).
11. Kim, C.H., Witherden, D.A. & Havran, W.L. Characterization and TCR variable region gene use of mouse resident nasal γδ T lymphocytes. *J. Leukoc. Biol.* **84**, 1259–1263 (2008).
12. Yin, Y. *et al.* An FGF-WNT gene regulatory network controls lung mesenchyme development. *Dev. Biol.* **319**, 426–436 (2008).
13. Yin, Y., Wang, F. & Ornitz, D.M. Mesothelial- and epithelial-derived FGF9 have distinct functions in the regulation of lung development. *Development* **138**, 3169–3177 (2011).
14. Chen, D., Jarrell, A., Guo, C., Lang, R. & Atit, R. Dermal β-catenin activity in response to epidermal Wnt ligands is required for fibroblast proliferation and hair follicle initiation. *Development* **139**, 1522–1533 (2012).
15. Ornitz, D.M. *et al.* Receptor specificity of the fibroblast growth factor family. *J. Biol. Chem.* **271**, 15292–15297 (1996).
16. Hendrix, N.D. *et al.* Fibroblast growth factor 9 has oncogenic activity and is a downstream target of Wnt signaling in ovarian endometrioid adenocarcinomas. *Cancer Res.* **66**, 1354–1362 (2006).

17. Ebert, L.M., Meuter, S. & Moser, B. Homing and function of human skin γδ T cells and NK cells: relevance for tumor surveillance. *J. Immunol.* **176**, 4331–4336 (2006).
18. Bos, J.D. *et al.* T cell receptor γδ bearing cells in normal human skin. *J. Invest. Dermatol.* **94**, 37–42 (1990).
19. Bos, J.D. *et al.* The skin immune system (SIS): distribution and immunophenotype of lymphocyte subpopulations in normal human skin. *J. Invest. Dermatol.* **88**, 569–573 (1987).
20. Foster, C.A. *et al.* Human epidermal T cells predominantly belong to the lineage expressing α/β T cell receptor. *J. Exp. Med.* **171**, 997–1013 (1990).
21. Gray, E.E., Suzuki, K. & Moser, J.G. Identification of a motile IL-17–producing γδ T cell population in the dermis. *J. Immunol.* **186**, 6091–6095 (2011).
22. Clark, R.A. *et al.* The vast majority of CLA^+ T cells are resident in normal skin. *J. Immunol.* **176**, 4431–4439 (2006).
23. Huelsken, J., Vogel, R., Erdmann, B., Cotsarelis, G. & Birchmeier, W. β-catenin controls hair follicle morphogenesis and stem cell differentiation in the skin. *Cell* **105**, 533–545 (2001).
24. Zhang, Y. *et al.* Reciprocal requirements for EDA/EDAR/NF-κB and Wnt/β-catenin signaling pathways in hair follicle induction. *Dev. Cell* **17**, 49–61 (2009).
25. Reddy, S. *et al.* Characterization of *Wnt* gene expression in developing and postnatal hair follicles and identification of *Wnt5a* as a target of Sonic hedgehog in hair follicle morphogenesis. *Mech. Dev.* **107**, 69–82 (2001).
26. Huang, S. *et al.* Wls is expressed in the epidermis and regulates embryonic hair follicle induction in mice. *PLoS ONE* **7**, e45904 (2012).
27. Wells, K.L. *et al.* Genome-wide SNP scan of pooled DNA reveals nonsense mutation in FGF20 in the Scaleless line of featherless chickens. *BMC Genomics* **13**, 257 (2012).
28. Widelitz, R.B., Jiang, T.X., Lu, J. & Chuong, C.M. β-catenin in epithelial morphogenesis: conversion of part of avian foot scales into feather buds with a mutated β-catenin. *Dev. Biol.* **219**, 98–114 (2000).
29. Huh, S.H. *et al.* Fgf20 governs formation of primary and secondary dermal condensations in developing hair follicles. *Genes Dev.* **27**, 450–458 (2013).
30. Livak, K.J. & Schmittgen, T.D. Analysis of relative gene expression data using real-time quantitative PCR and the $2^{-\Delta\Delta C_t}$ method. *Methods* **25**, 402–408 (2001).

ONLINE METHODS

Mice. The following transgenic and knockout mice have been described previously: FVB-Tg(KRT14-rtTA)F42Efu/J (K14rtTA) mice[31], TRE-*Fgf9*-IRES-*EGFP* mice[32], *Fgf9*$^{fl/fl}$ mice[33], *Axin2-LacZ* heterozygous reporter mice[34], *Krt14-Wnt7a* mice[1] and Tcrd-H2BEGFP mice[8]. We purchased C57BL/6 control mice (stock 000664), *Lck-Cre* mice (stock 003802) and *Tcrd*$^{-/-}$ mice (stock 002120) from The Jackson Laboratory. Mice were housed in conventional, pathogen-free facilities at the animal facility of the University of Pennsylvania School of Medicine. The Institutional Animal Care and Use Committee at the University of Pennsylvania reviewed and approved all mouse protocols.

Human tissue. We obtained normal skin from patients undergoing abdominoplastic or mammary reduction surgery through the Cooperative Human Tissue Network with University of Pennsylvania Institutional Review Board review and approval and written informed consent by all patients.

Wounding and wound-induced hair neogenesis analyses. We excised full-thickness skin from the backs of mice under isoflurane anesthesia as previously described[35]. Mice aged 6–8 weeks received 1.2 × 1.2 cm^2 full-thickness excision wounds in all experiments. K14rtTA; TRE-*Fgf9*-IRES-*EGFP* interbred mice and controls received doxycycline food, and *Lck-Cre*; *Fgf9*$^{fl/fl}$ interbred mice and controls received intraperitoneal injections of tamoxifen (1 mg per mouse) during the final week of wound healing (PWD9–PWD16).

Healed skin was taken 9–14 d after reepithelialization and epidermis and dermis separated using 20 mM EDTA or dispase as described[1]. Epidermal K17 immunostaining (1:5,000, rabbit polyclonal antisera provided by P. Coulombe) and dermal nitroblue tetrazolium/5-bromo-4-chloro-3′-indolyphosphate *p*-toluidine (NBT/BCIP) staining were done to identify new hair germs and follicular dermal papillae in wounds as previously described[1].

Fgf9 antibody and Fgf9-adenovirus experiments in adult mice. We injected 50 µl of 10 µg ml^{-1} anti-Fgf9 (R&D MAB273) or a mouse IgG2a isotype control antibody (clone UPC-10, Sigma-Aldrich) daily into wound dermis during late healing (PWD12–PWD16) and counted new hair follicles 10–14 d later.

The pGEM-Fgf9 plasmid, provided by D.M.O., served as a template for PCR amplification of the *Fgf9* coding sequence. Recombinant adenovirus was generated according to methodology described by Shi *et al.*[36].

Whole-mount assays to detect β-galactosidase activity. To detect β-galactosidase activity, wound tissue (dermis and epidermis) was treated as described[1], photographed and frozen in optimal cutting temperature (OCT) medium at −80 °C in preparation for cryosectioning.

Antibodies. Antibodies used in these studies included antibodies specific for β-catenin (1:100, clone 14, BD Biosciences), Ki-67 (1:100, clone B56, BD Biosciences), CD45 (1:100, clone 30-F11, BD Biosciences), CD31 (1:100, clone MEC 13.3, BD Biosciences), γδ TCR (1:100, clone GL3, BD Biosciences), TCR Vγ2 (1:50, UC3-10A6), TCR-β (1:100, clone H57-597, BD Biosciences), CD3 (1:100, clone 145-2C11, eBioscience), human CD3 (1:20, clone HIT3a, BioLegend), human γδ TCR (1:40, clone 5A6.E9, Thermo Scientific) and human CD31 (1:100, clone MBC 78.2, Invitrogen).

Immunofluorescence and quantification of γδ T cells in human and mouse frozen sections and *in situ* analyses. Tissue, flash frozen in OCT medium at −80 °C, was cryosectioned and typically fixed with 4% paraformaldehyde. In mouse skin, for detection of external antigens, we blocked tissue in 5% FCS in PBS and then incubated with the appropriate antibodies overnight at 4 °C, washed and then refixed tissue. For detection of intracellular antigens, we permeabilized sections with 0.5% Triton X-100, then incubated with the appropriate antibodies as described above. In human skin, for detection of CD3, TCRδ chain and CD31, we stained unfixed frozen sections with antibodies for 1 h followed by brief staining with secondary antibodies and then fixation. To determine percentages of CD3$^+$γδ$^-$ cells (CD3$^+$TCRδ$^-$) and γδ$^+$ T cells (CD3$^+$TCRδ$^+$) in frozen sections, we manually counted stained cells and all DAPI$^+$ nuclei within the dermis of a section, divided stained cell numbers from DAPI$^+$ cell numbers and multiplied by 100. For *in situ* analyses, tissue sections were first photographed to determine location of GFP$^+$ cells. We then subjected tissue to *in situ* analyses for detection of *Fgf9* transcripts according to the method of Braissant and Wahli[37] and rephotographed. *Fgf9* sense and antisense probes were generated from a pFgf9 template using the DIG RNA labeling kit SP6/T7 (Roche). The T7 sense control showed no staining (**Supplementary Fig. 7b**).

Cell collection, FACS analyses and cell sorting for qPCR and CDR3 sequencing. We separated wound or normal epidermis and dermis as described[1]. To generate single-cell suspensions for FACS and cell sorting, epidermis was further incubated with 0.25% trypsin in EDTA with mechanical dissociation at 37 °C for 5 min. Dermis was diced and incubated with 3 mg ml^{-1} collagenase in PBS at 37°C for 1 h. Dissociation of human dermal cells required 4–5 h incubation with rotation. Cells were counted, incubated with Fc block (BD Biosciences) and then antibodies. We undertook FACS analyses using a FACSCanto A and cell sorting using FACSVantage scanning electron microscopy and FACSDiVa software and analyzed data using FlowJo software. We sorted populations with low cell numbers directly into TRIzol LS (Life Technologies). To establish veracity of the sorting method for enrichment of wound fibroblasts used in **Figure 5**, we subjected the sorted populations (CD45$^+$, CD31$^+$ and double-negative fibroblasts) to qPCR using a panel of probes specific for each population (**Supplementary Fig. 6**). The fibroblast population was found to express high amounts of the fibroblast-specific *Col1a2* and *Pdgfra* but not T cell, antigen-presenting cell or endothelial cell transcripts.

PCR, quantitative real-time PCR and CDR3 sequence analyses. We isolated RNA from whole tissue or sorted cells using the RNeasy microkit (Qiagen) and assessed RNA concentration using a Nanodrop 2000c spectrophotometer (Thermo Scientific). Roughly equal amounts of RNA were converted to cDNA using the Superscript First-Strand Synthesis System (Invitrogen). PCR analyses to investigate Vγ use by γδ T cells were done using primer sets described by Andrew *et al.*[38]. QPCR was done using a StepOnePlus Real-Time PCR System (Applied Biosystems) with Taqman primer and probe sets from Applied Biosystems. We performed reactions in triplicate and standardized relative expression levels using housekeeping genes *Actb* or 18S rRNA as internal controls. Results were obtained by the comparative C_t method using the StepOne software program with derivations defined by Livak and Schmittgen[30] and expressed as fold change with respect to the experimental control *Actb* or 18S rRNA. For CDR3 analyses, we amplified cDNA from sorted ear dermal Vγ2$^-$ cells using Vγ1.1, Vγ4 or Vδ1 primers defined by Andrew *et al.*[40]. Resultant PCR products were cloned into TOPO vectors (Invitrogen) and sequenced.

Fibroblast culture experiments. We collected PWD10 dermis and generated single-cell suspensions as described above. We cultured 1 × 10^5 cells in DMEM with 10% FCS and penicillin-streptomycin for 24 h, then washed to remove nonadherent cells and recultured with rFgf9 (Abcam) or rWnt2 (R&D) at varying concentrations and times as described in **Figure 5**. Culture supernatants were subjected to ELISA for detection of Fgf9 (Abcam Fgf9 ELISA kit). Cells were harvested in TRIzol LS reagent and processed for RNA for qPCR as described above.

Statistical analyses. All statistical analyses were done by two-tailed Student's *t* test using Excel (Microsoft). $P < 0.05$ was considered significant. All data are expressed as means ± s.e.m.

31. Nguyen, H., Rendl, M. & Fuchs, E. Tcf3 governs stem cell features and represses cell fate determination in skin. *Cell* **127**, 171–183 (2006).
32. White, A.C. *et al.* FGF9 and SHH signaling coordinate lung growth and development through regulation of distinct mesenchymal domains. *Development* **133**, 1507–1517 (2006).
33. Lin, Y., Liu, G. & Wang, F. Generation of an *Fgf9* conditional null allele. *Genesis* **44**, 150–154 (2006).
34. Lustig, B. *et al.* Negative feedback loop of Wnt signaling through upregulation of conductin/axin2 in colorectal and liver tumors. *Mol. Cell Biol.* **22**, 1184–1193 (2002).
35. Ito, M. *et al.* Stem cells in the hair follicle bulge contribute to wound repair but not to homeostasis of the epidermis. *Nat. Med.* **11**, 1351–1354 (2005).
36. Shi, G. *et al.* Expression of paired-like homeodomain transcription factor 2c (PITX2c) in epidermal keratinocytes. *Exp. Cell Res.* **316**, 3263–3271 (2010).
37. Braissant, O. & Wahli, W. A simplified *in situ* hybridization protocol using non–radioactively labeled probes to detect abundant and rare mRNAs on tissue sections. *Biochemica* **1**, 11–16 (1998).
38. Andrew, E.M. *et al.* Delineation of the function of a major γδ T cell subset during infection. *J. Immunol.* **175**, 1741–1750 (2005).